Estimating the State-of-Charge of Lithium-Ion Batteries Using an H-Infinity Observer with Consideration of the Hysteresis Characteristic

Jiale Xie[*], Jiachen Ma[†], Yude Sun[**], and Zonglin Li[**]

[*,†]School of Astronautics, Harbin Institute of Technology, Harbin, China
[**]School of Information Science and Engineering, Harbin Institute of Technology at Weihai, Weihai, China

Abstract

The conventional methods used to evaluate battery state-of-charge (SOC) cannot accommodate the chemistry nonlinearities, measurement inaccuracies and parameter perturbations involved in estimation systems. In this paper, an impedance-based equivalent circuit model has been constructed with respect to a $LiFePO_4$ battery by approximating the electrochemical impedance spectrum (EIS) with RC circuits. The efficiencies of approximating the EIS with RC networks in different series-parallel forms are first discussed. Additionally, the typical hysteresis characteristic is modeled through an empirical approach. Subsequently, a methodology incorporating an H-infinity observer designated for open-circuit voltage (OCV) observation and a hysteresis model developed for OCV-SOC mapping is proposed. Thereafter, evaluation experiments under FUDS and UDDS test cycles are undertaken with varying temperatures and different current-sense bias. Experimental comparisons, in comparison with the EKF based method, indicate that the proposed SOC estimator is more effective and robust. Moreover, test results on a group of Li-ion batteries, from different manufacturers and of different chemistries, show that the proposed method has high generalization capability for all the three types of Li-ion batteries.

Key words: H-infinity observer, Hysteresis characteristic, Impedance-based modeling, State-of-charge

I. INTRODUCTION

Lithium-ion battery related technologies have been attracting the interest of modern electric vehicle producers because of their high specific energy and long lifetime compared to lead-acid and nickel-metal batteries [1]-[2]. To prevent permanent damage and to enable optimum use of the battery, regular operating conditions should be guaranteed by the battery energy management system (BEMS). The accurate and reliable estimation of the State-of-Charge (SOC) is an essential prerequisite for BEMSs to determine the energy management strategy [3]. Nevertheless, the inherent charge-discharge processes involve complex electrochemical kinetics inside the battery and as an internal state the SOC is generally unmeasurable. Consequently, some relevant

quantities need to be measured to identify the SOC indirectly.

Several techniques and methods have been reported to improve SOC estimation performance. Although the charge counting method [4] is simple to utilize, the determination of the initial SOC is difficult and errors caused by uncertain noise, sensor resolution and measurement rounding are increasingly accumulated. The open-circuit-voltage (OCV) method [5] needs to deactivate the battery untill the terminal voltage approaches its equilibrium potential. In addition, the very flat OCV-SOC plateau and the pronounced hysteresis phenomenon during the operation range (the solid ellipse marked area in Fig. 1) make precise assessment of the SOC very complicated. The Kalman filter method was put forward to perform closed-loop SOC estimation in ideal linear systems [6]. To adapt to nonlinear models (the dash ellipses marked areas in Fig. 1), the Extended Kalman filter (EKF) [7] and the Unscented Kalman Filter (UKF) [8] were employed. However, they give unreliable results in the presence of severe nonlinearities and the performance is sensitive to the assumptions of noise characteristics. When the system and measurement noises are non-Gaussian or correlated, the filters
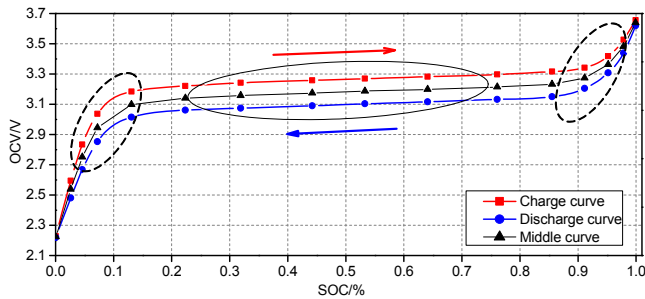
Fig. 1. Schematic illustration of OCV-SOC relationship during continuous charging and discharging process respectively.
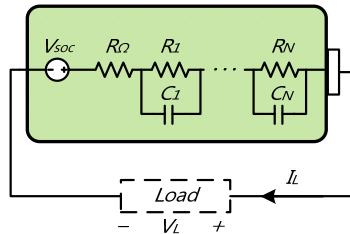

Fig. 2. A typical equivalent circuit model framework for batteries, N denotes the order of RC-ladders.

are suboptimal [9]. Arising from temperature fluctuations, current alternations and aging, there inevitably exist uncertainties in battery models, which might result in performance deterioration, even system divergence. In order to address these problems, attempts to assess the SOC with observer-based techniques have been documented [10]. As a robust filter, the H∞ observer based SOC evaluation method [11] not only guarantees system stability, but also maintains good adaptability and great robustness.

SOC estimation algorithms are commonly applied in conjunction with appropriate battery models. Some studies were carried out on electrochemical models from the perspective of a molecular level [12]. Since it is necessary to rely on readily available measurements such as instantaneous terminal voltage and current, the chemistry-dependent models are not applicable. Neural network based models [7] possess superior capability in terms of nonlinear fitting. Nevertheless, the training of neural networks is time-consuming and relies heavily on adequate historical data to completely model the dynamic behavior so as to attain acceptable generalization capability. Equivalent circuit models [13] are another common category for battery modeling. Typically, an equivalent series resistor (ESR) is used as the battery internal resistance (constant or varying with the SOC and temperature), a voltage source as the OCV or a bulk capacitor as the capacity. For the sake of reproducing the primary electrical characteristic, high order RC networks are incorporated as illustrated in Fig. 2, where N denotes the order of the RC ladders. In the frequency domain, electrochemical impedance spectroscopy (EIS) has been introduced either to figure out the SOC directly [14], or as an effective approach for battery modeling [15]. Additionally,

TABLE I
SPECIFICATIONS OF THE INVESTIGATED LPF LI-ION BATTERY

Parameter	Value	Unit
Manufacturer	HUANYU NEW ENERGY	
Nominal capacity	10 (0.3C discharge)	Ah
Nominal voltage	3.2	V
Upper cut-off voltage	3.65	V
Lower cut-off voltage	2.2	V
Operating temperature	Charge:0~45 Discharge:-20~60	℃

Fig. 3. Dedicated battery charge-discharge tester (left), thermally controlled environmental chamber (middle) and electrochemical impedance spectroscopy instrument (right).

since regenerative braking is widely adopted in electric vehicles, frequent alterations between charging and discharging are common scenarios during vehicle operation. Thus, the hysteresis phenomenon has been taken into consideration in battery modeling [16].

The remainder of this paper is structured as follows. In section II, the investigated battery and the equipment for testing are introduced. An equivalent circuit model is built by approximating the impedance spectrum with RC networks in the frequency domain, and the OCV-SOC relationship is identified with consideration of the hysteresis effect. The procedure of the proposed SOC estimation scheme and a detailed theoretical analysis of the H∞ observer designated for OCV observation are depicted subsequently. In the following section, the proposed battery model is evaluated through a comparison between the measured and the simulated voltage responses in the time domain. Then experimental details of a practical implementation using the proposed methodology, in comparison with the EKF-based one, verify the effectiveness of the proposed method. Additionally, to check the generalization capability of the proposed method, several other batteries, from different manufacturers and of different cathode materials, are tested. Finally, some conclusions are drawn and future works are discussed.

II. MATERIALS AND METHODS

A. Investigated Battery and Equipment

This research work has been conducted on a 10Ah LiFePO$_4$ (LFP) battery, the specifications of which are listed in Table I.

A dedicated battery tester, as shown in Fig. 3 (left), is mandatory to perform charge-discharge experiments under various current profiles. The ambient temperature is a remarkable factor that influences the battery electrical properties. During the experiment, the battery is contained in a thermally controlled chamber, as presented in Fig. 3 (middle), to provide pre-set environmental conditions. When measuring the EIS of the battery, small-signal excitations (lower than 10mV) within the specified frequency range are applied on the cell while simultaneously evaluating its response with an *EISmeter*, which is shown in Fig. 3 (right).

B. Battery Modeling

1) Impedance-based Equivalent Circuit Model

As an analytic method in the frequency domain, the EIS of a battery characterizes its dynamic behavior. Therefore, it is usually employed for equivalent circuit parameterization. In this paper, impedance measurements of the battery were obtained with an *EISmeter* under the conditions that SOC=70%, discharge rate=1C, ambient temperature=25℃ and frequency from 0.1 to 0.5k HZ. The acquired original impedance diagram has been ploted in the *Nyquist* plane as presented in Fig. 4 (the black line with solid square marks, the negative imaginary part vs. the real part), characterizing an oblate semicircle at the high-frequency stage and a fixed gradient line at the low-frequency stage. Then the original impedance spectrum is fitted with the circuits shown in Fig. 2 by *ZSimpWin*, where N denotes the order of the RC ladders. Obviously, as N increases, the fitted curve gradually approaches to the original curve as depicted in Fig. 4. As a tradeoff between complexity and accuracy, $N = 3$ is chosen in this paper.

In order to study the approximation efficiency by different circuits on the impedance characteristics, several circuit variations, referring to the *Thevenin* model [13] and the *Saft Capacitance* model [17], are evaluated. Fig. 5 (b) describes four 3rd-order heteroid RC circuits in different series-parallel forms used for fitting. As Fig. 5 (a) depicts, the fitting differences between the four circuits are negligible, i.e., all four of he circuit forms apply to the impedance spectrum approximation.

To obtain the observable system state-space expression, an equivalent circuit formed as R(R(RC)(RC)(RC)), as shown in Fig. 5 (b), is adopted referring to [17]. The amount of stored energy can be denoted as a bulk capacitor C_{bulk}. The capacitance of C_{bulk} can be calculated by Equ. (1), where $V_{(100\%SOC)}$ and $V_{(0\%SOC)}$ are the OCV at corresponding SOC points. C_N is the nominal capacity in Amp·Sec. Since the value of C_{bulk} is fixed, the values of the remaining components can be given by *Zsimpwin* by fitting the impedance spectrum.

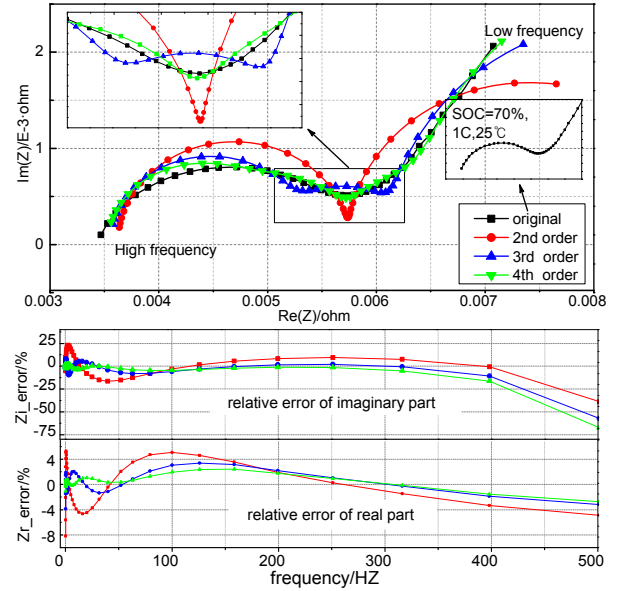$$C_{bulk} = \frac{C_N \cdot V_{100\%SOC}}{(V_{100\%SOC}^2 - V_{0\%SOC}^2)/2} \tag{1}$$

Fig. 4. Results of fitting the impedance spectrum of the investigated battery with 2nd-, 3rd- and 4th-order series RC circuit respectively (shaped like Fig. 2, *N*=2, 3, 4 respectively).
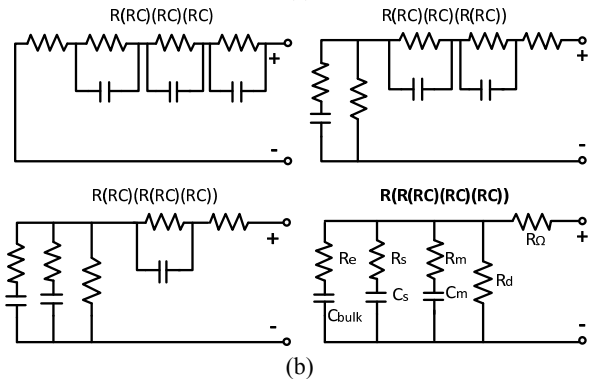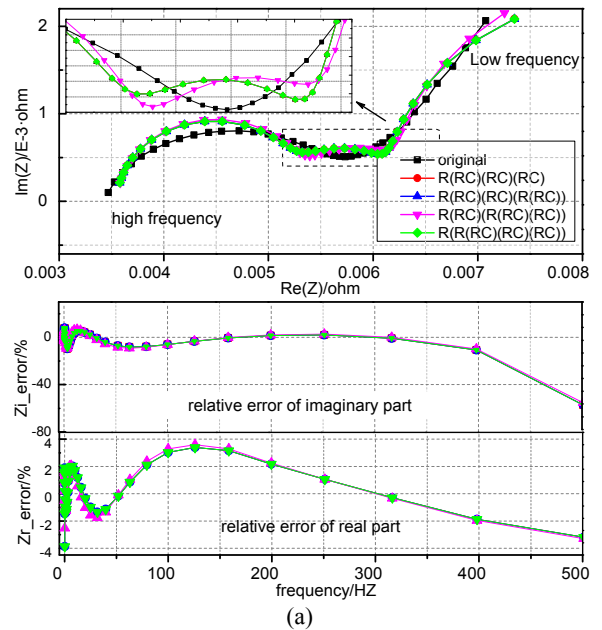

Fig. 5. Results of fitting the impedance spectrum with different RC circuits. (a) original spectrum and fitting results. (b) 3rd-order heteroid circuits used for fitting.
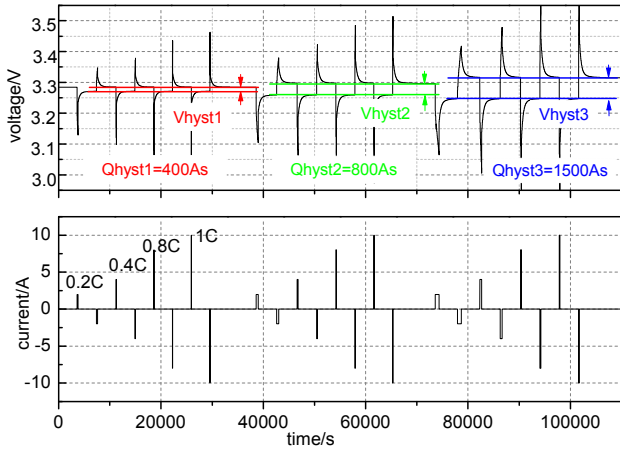
Fig. 6. The response of applying alternating pulses at various current rates but with a constant amount of charge per pulse (400As, 800As and 1500As respectively) and rest durations of 3600s in between on the Li-ion cell.

2) Determination of the OCV-SOC Relationship

The OCV of Li-ion batteries is not determined solely by the SOC. However, it is relevant to the pretreatments due to the complex electrochemical reactions, e.g. the hysteresis phenomenon has significant impacts on the OCV-SOC relationship (Fig. 1). According to the findings on NiMH batteries outlined in [15], that the hysteresis voltage (V_{hyst}) depends exclusively on the throughput of ampere hours (Q_{hyst}) in the charging or discharging course, similar research and further study have been carried out on the LiFePO$_4$-based battery in this paper. As shown in Fig. 6, alternating pulses at various rates (0.2C, 0.4C, 0.8C and 1.5C) but with a constant amount of charge per pulse (400As, 800As and 1500As, respectively) and rest durations of 3600s in between for equilibrium potential recovery are applied to the Li-ion cell. The gaps (V_{hyst}) between the horizontal colored lines are independent of the current rate, but correspond to the throughput of the transferred charge (Q_{hyst}). Accordingly, it is reasonable to conclude that the finding in [15] turns out to be applicable to the LPF battery. Additionally, it is found that the maximum of Q_{hyst} (Q_{hyst_max}, $A \rightarrow B$ in Fig. 7) remains as a constant (approximately equals to $0.042 \cdot C_N$) and that the charging semicycle and discharging semicycle of the inner hysteresis curves are symmetric and similarly shaped during the operation range (10%-90% SOC).

Three different hysteresis cases are portrayed in Fig. 7. Case1 ($A \rightarrow B \rightarrow A$) illustrates a typical hysteresis cycle with a charge throughput of Q_{hyst_max} and both of the terminal points just locate on the upper and lower OCV-SOC boundaries respectively; Case2 ($A \rightarrow C \rightarrow A$ or $B \rightarrow C' \rightarrow B$) delineates shallow micro-cycles where the transferred charge is smaller than Q_{hyst_max}; Case3 ($A \rightarrow B \rightarrow B' \rightarrow A' \rightarrow A$) is a deep hysteresis cycle and it describes the procedure of continuously charging with a charge amount over Q_{hyst_max} and then discharging to the lower boundary. All three cases
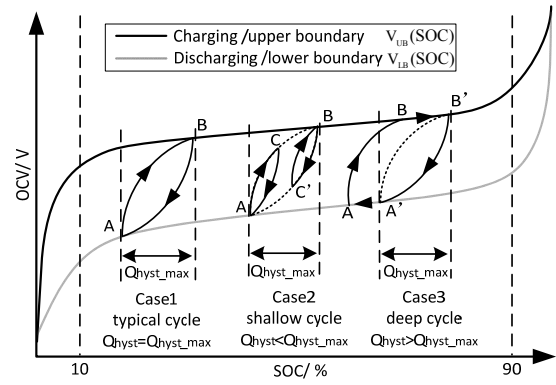

Fig. 7. Three different hysteresis inner cycles of equilibrium potential between the outer boundaries.
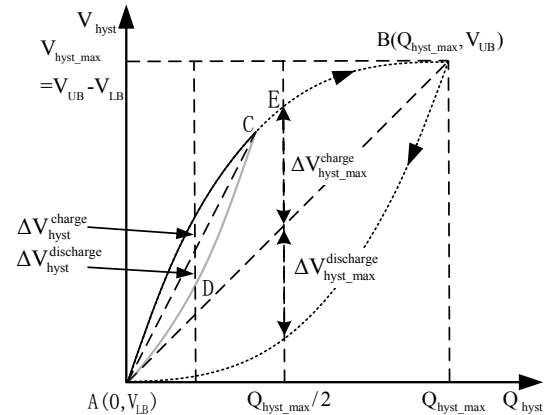

Fig. 8. Schematic of the zoomed-in hysteresis cycle in Fig. 7.

elucidate a core principle that, point B is always regarded as the relative reference target for the charging process, and point $A(A')$ is regarded as the relative reference target for the discharging process. From the observation of Fig. 7, the OCV can be regarded as the superimposition of $V(SOC)$ in the discharging course and hysteresis voltage, i.e. $OCV = V_{LB}(SOC) + V_{hyst}(Q_{hyst})$.

As Fig. 7 and 8 indicate, three prerequisites are mandatory for identifying the inner hysteresis trajectory.

a) The Outer Boundaries of the SOC-OCV Relationship

In essence, the actual variable corresponding to the SOC is the electromotive force (EMF) which is a crucial internal state of batteries. Because of the immeasurability of EMF, the open-circuit-voltage (OCV) is commonly used as a substitution in practical applications. The battery terminal voltage can be measured as OCV when the relax time $t \rightarrow \infty$ after the load is cut off. However, $t \rightarrow \infty$ is obviously infeasible. Thus, $t = 2000s$ is adopted and has been proven to be sufficient for equilibrium potential reestablishment by experiments. Thereafter, the boundary curves ($V_{LB}(SOC)$ and $V_{UB}(SOC)$) can be acquired through a cubic spline interpolation of the measured OCV-SOC point pairs both in charging and discharging course.

b) The Maximum of Transferred Charge in the Typical Hysteresis Semicycle (Q_{hys_max})
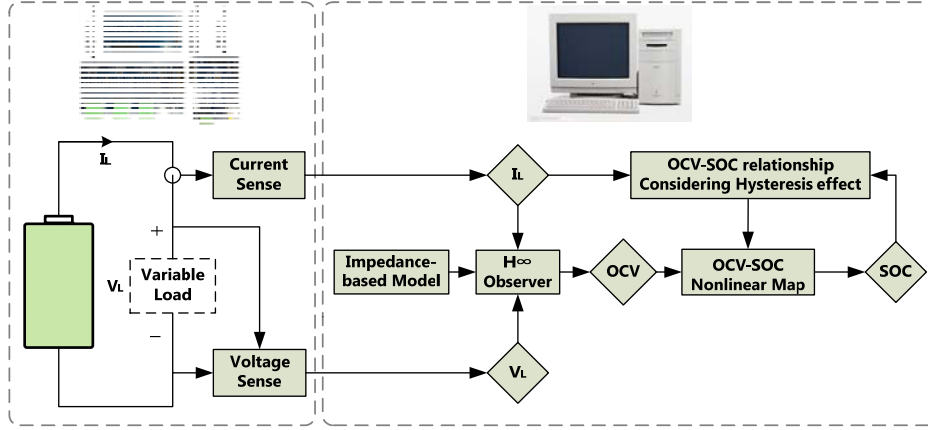
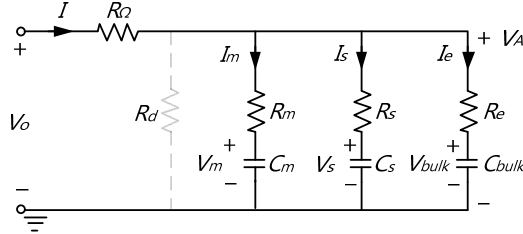Fig. 9. Schematic illustration of the proposed SOC estimation methodology.

Fig. 10. Simplified form of the electrical circuit for state-space expression with self-discharge resistor omitted.

By analyzing the experimental results, the maximum of the transferred charge Q_{hyst_max} in a complete (typical) hysteresis semicycle (Fig. 7 case1) remains a constant during the operation range (10%-90%SOC). For the investigated LPF battery, Q_{hyst_max} approximately equal to $0.042 \cdot C_N$ (1512As here).

c) *The Maximum of Hysteresis Voltage in Shallow Cycles (ΔV_{hyst}^{charge} and $\Delta V_{hyst}^{discharge}$)*

The values of $\Delta V_{hyst\_max}^{charge}$ and $\Delta V_{hyst\_max}^{discharge}$ can be derived by Equ. (2) at $Q_{hyst} = Q_{hys\_max}/2$, where η_{charge} and $\eta_{discharge}$ are the proportionality coefficients and SOC $\in$ [0.1,0.9].

$$\Delta V_{hyst\_max}^{charge} = (V_{UB}(SOC) - V_{LB}(SOC)) \times \eta_{charge}$$
$$\Delta V_{hyst\_max}^{discharge} = (V_{UB}(SOC) - V_{LB}(SOC)) \times \eta_{discharge}$$
(2)

According to experimental measurements, η_{charge} and $\eta_{discharge}$ can be set as 0.247 and 0.218, respectively. Referring to [15], the correlation between ΔV_{hyst}^{charge} and $\Delta V_{hyst\_max}^{charge}$ ($\Delta V_{hyst}^{discharge}$ and $\Delta V_{hyst\_max}^{discharge}$) can be expressed in Equ. (3).

$$\Delta V_{hyst}^{discharge} = \Delta V_{hyst\_max}^{discharge} \frac{Q_{hyst}}{Q_{hyst\_max}}$$
$$\Delta V_{hyst}^{charge} = \Delta V_{hyst\_max}^{charge} \frac{Q_{hyst\_max} - Q_{hyst}}{Q_{hyst\_max}}$$
(3)

Taking the shallow hysteresis cycle ($A \rightarrow C \rightarrow A$) in Fig. 8 as an example, when the cell is charged from the start point A on the lower boundary, the corresponding target point B on the upper boundary can be determined by Q_{hyst_max}

($SOC_B = SOC_A + Q_{hyst\_max}/C_N$). C is the stochastic endpoint of the charging process depending on the load. The charging trace of the equilibrium potential ($A \rightarrow C$) overlaps with the typical hysteresis charging semicycle ($A \rightarrow C \rightarrow E \rightarrow B$), which can be obtained using a 2nd-order polynomial approximation of points A, B and E (regarding E as the pole of the charging semicycle at $Q_{hyst} = Q_{hyst\_max}/2$). Similarly, the discharging trace ($C \rightarrow D \rightarrow A$) can be worked out by regarding C as the start point, A as the end point and D as the pole.

C. H∞ Based Observer for OCV Observation

The H∞ observer does not require information on the noise characteristics and provides consistent performance when subject to uncertainties and disturbances. For the purpose of accommodating mode uncertainties due to current, temperature and aging, a linear robust H∞ observer was designated to perform OCV observation. The schematic diagram in Fig. 9 demonstrates the procedure of the proposed methodology, where the H∞ observer determines the OCV and the OCV-SOC relationship model (studied in section II.B.2) ultimately gives the SOC estimation result.

The electrical significance of R_d in R(R(RC)(RC)(RC)) form (Fig. 5 (b)) is the self-discharge resistor. Accounting for that the resistance of R_d (usually in the level of 10^8) is considerably larger than other resistors, the self-discharge impact on the transient response can be ignored. Thereafter, R(R(RC)(RC)(RC)) is simplified as Fig. 10 with R_d omitted.

According to *Kirchhoff* laws and knowledge of transient circuits, the following equations can be derived:

$$V_0 = IR_\Omega + V_A \tag{4}$$

$$I_e = (V_A - V_{bulk})/R_e \tag{5}$$

$$I_s = (V_A - V_s)/R_s \tag{6}$$

$$I_m = (V_A - V_m)/R_m \tag{7}$$

$$I_e = C_{bulk}\dot{V}_{bulk} \tag{8}$$

$$I_s = C_s\dot{V}_s \tag{9}$$

$$I_m = C_m \dot{V}_m \qquad (10)$$

$$I = I_m + I_s + I_e \qquad (11)$$

From Equs. (5)-(7) and (11), V_A can be easily deduced as

$$V_A = \frac{I R_e R_s R_m + V_{bulk} R_s R_m + V_s R_e R_m + V_m R_e R_s}{R_s R_m + R_e R_m + R_e R_s}. \qquad (12)$$

Combining Equs. (6)-(8) and (11)-(12), the expression of the voltage across the bulk capacitor C_{bulk} can be rewritten:

$$\dot{V}_{bulk} = \frac{I R_m R_s}{\alpha C_{bulk}} - \frac{V_{bulk}(R_m + R_s)}{\alpha C_{bulk}} + \frac{V_m R_s}{\alpha C_{bulk}} + \frac{V_s R_m}{\alpha C_{bulk}}, (13)$$

where $\alpha = R_e R_m + R_e R_s + R_m R_s$.

Similarly, $\dot{V}_s$ and $\dot{V}_m$ can be derived as (14) and (15).

$$\dot{V}_s = \frac{I R_e R_m}{\alpha C_s} - \frac{V_s(R_m + R_e)}{\alpha C_s} + \frac{V_m R_s}{\alpha C_s} + \frac{V_{bulk} R_m}{\alpha C_s}, \quad (14)$$

$$\dot{V}_m = \frac{I R_e R_s}{\alpha C_m} - \frac{V_m(R_e + R_s)}{\alpha C_m} + \frac{V_{bulk} R_s}{\alpha C_m} + \frac{V_s R_e}{\alpha C_m}. \quad (15)$$

From Equ. (4) and (12) the terminal voltage is obtained as:

$$V_0 = I\left(R_\Omega + \frac{\beta}{\alpha}\right) + \frac{R_e R_m}{\alpha} V_s + \frac{R_e R_s}{\alpha} V_m + \frac{R_s R_m}{\alpha} V_{bulk} \quad (16)$$

where $\beta = R_e R_m R_s$.

The system state variables are chosen as $x(t) = [V_s \quad V_m \quad V_{bulk}]^T$, and the system input and output are selected as $u(t) = I$ and $y(t) = V_0$, respectively. Therefore, the state-space equations can typically be expressed as:

$$\begin{cases} \dot{x}(t) = Ax(t) + Bu(t) \\ y(t) = Cx(t) + Du(t) \end{cases} \qquad (17)$$

where:

$$A = \begin{bmatrix} -\dfrac{R_m + R_e}{\alpha C_s} & \dfrac{R_e}{\alpha C_s} & \dfrac{R_m}{\alpha C_s} \\ \dfrac{R_e}{\alpha C_m} & -\dfrac{R_s + R_e}{\alpha C_m} & \dfrac{R_s}{\alpha C_m} \\ \dfrac{R_m}{\alpha C_{bulk}} & \dfrac{R_s}{\alpha C_{bulk}} & -\dfrac{R_s + R_m}{\alpha C_{bulk}} \end{bmatrix}, B = \begin{bmatrix} \dfrac{R_e R_m}{\alpha C_s} \\ \dfrac{R_e R_s}{\alpha C_m} \\ \dfrac{R_m R_s}{\alpha C_{bulk}} \end{bmatrix},$$

$$C = \begin{bmatrix} \dfrac{R_e R_m}{\alpha} & \dfrac{R_e R_s}{\alpha} & \dfrac{R_s R_m}{\alpha} \end{bmatrix}, D = \begin{bmatrix} R_\Omega + \dfrac{\beta}{\alpha} \end{bmatrix}.$$

Owing to complex internal chemical reactions and outer interferences such as EMI, there definitely exist system uncertainties and measurement noises in the actual behavior of the cell. With reasonable modifications, Equ. (17) is transformed to:

$$\begin{cases} \dot{x}(t) = Ax(t) + Bu(t) + E\omega_0(t) \\ y(t) = Cx(t) + Du(t) + F\omega_0(t) \end{cases} \qquad (18)$$

where $\omega_0(t) = [\eta \quad \omega]^T$ is the noise matrix, the forms of E, F are as $E = [I_{n*n} \quad 0_{n*q}]$, $F = [0_{1*n} \quad I_{1*q}]$, and n, q are the dimensions of x, y, respectively.

The observability of (A, C) can be analyzed by calculating the determinant of:

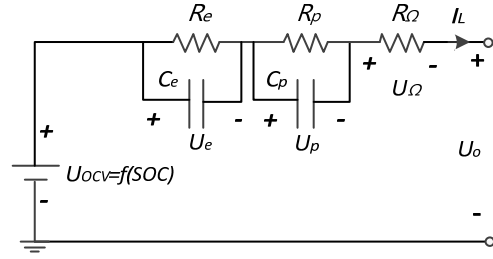$$Q_0 = [C \quad CA \quad CA^2]^T. \qquad (19)$$

Fig. 11. Equivalent circuit model for EKF based SOC estimation.

If Equ. (19) is nonsingular, then an H∞ observer of (A, C) can be designed as:

$$\begin{cases} \dot{\bar{x}}(t) = A\bar{x}(t) + Bu(t) + L(y - \bar{y}) \\ \bar{y}(t) = C\bar{x}(t) + Du(t) \end{cases} \qquad (20)$$

where L is the observer gain, and $\bar{x}(t)$ and $\bar{y}(t)$ are the estimates of $x(t)$ and $y(t)$. The system error equations are defined as:

$$\begin{cases} \dot{e}_x(t) = (A - LC)e(t) + (E - LF)\omega_0(t) \\ e_y(t) = Ce_x(t) + F\omega_0(t) \end{cases} \qquad (21)$$

where $e_x(t) = x(t) - \bar{x}(t)$, $e_y(t) = y(t) - \bar{y}(t)$.

According to [18]-[19], for Equs. (18) and (20), with the given attenuation level $\gamma > 0$, if there exist a positive definite matrix $P = P^T$ and an appropriate matrix X, such that the following linear matrix inequality is feasible:

$$\begin{bmatrix} AP + BX + (AP + BX)^T & E & (CP + DX)^T \\ E^T & -I & F^T \\ CP + DX & F & -\gamma^2 I \end{bmatrix} < 0, (22)$$

then it is possible to obtain an observer gain $L = P^{-1}X$ that satisfies:

- $\|e_x(t)\| \le \gamma\|\omega(t)\|$, which is the prescribed performance index under the zero initial condition;
- Error system (21) is stable.

First of all, the attenuation level γ needs to be deliberately determined. The following LMI *mincx* problem (the minimization of a linear objective under LMI constraints) can be solved to select an appropriate $\gamma = \sqrt{\upsilon}$.

$$\begin{aligned} &min(\upsilon) \\ s.t. &\begin{cases} P > 0 \\ \begin{bmatrix} AP + BX + (AP + BX)^T & E & (CP + DX)^T \\ E^T & -I & F^T \\ CP + DX & F & -\upsilon I \end{bmatrix} < 0 \end{cases} \end{aligned} . (23)$$

Then the attenuation level can be set as $\gamma^* = \gamma + \xi$, where ξ is an arbitrary stability margin. Finally, by solving Equ. (22), the matrices P, X and L can be confirmed.

D. EKF Based SOC Estimation

Based on the widely used *Thevenin* model [13], an improved one (Fig. 11) is obtained by adding an extra RC branch which represents the polarization characteristic. The hysteresis effect is not considered here and the U_{OCV} can be obtained by fitting the middle curve between the upper and
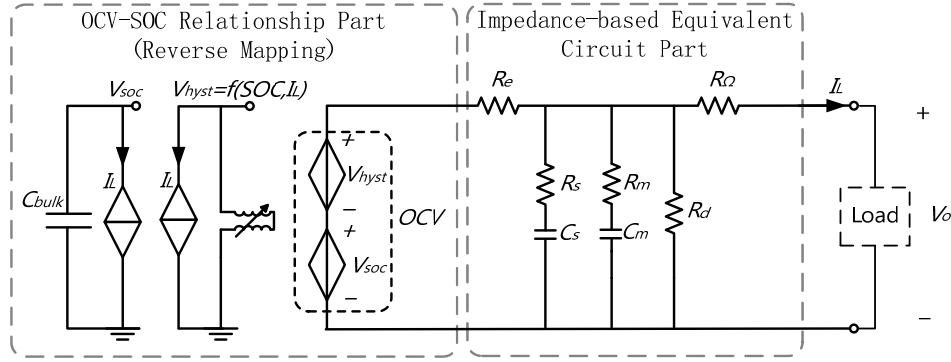
Fig. 12. The combined model of the investigated battery, incorporating equivalent circuit part and OCV-SOC relationship part.

lower boundaries (Fig. 1) with a 5th-order polynomial as:

$$U_{OCV} = f(SOC) = \sum_{n=0}^{N} a_n \cdot SOC^n, N = 5. \qquad (24)$$

The other parameters, R_e, R_p, R_Ω, C_e and C_p can be identified through the HPPC test in the time domain.

$x_k = [u_k^\Omega \quad u_k^e \quad u_k^p \quad SOC_k]^T$ and $y_k = U_k^o$ are chosen as the state and output variables, respectively. Then the state-space can be expressed in discrete form as:

$$\begin{cases} x_{k+1} = Ax_k + Bi_k + \omega_k \\ y_k = f(x_k) - u_k^\Omega - u_k^e - u_k^p + v_k \end{cases} \qquad (25)$$

where ω_k and v_k are the independent, zero mean, Gaussian process and measurement noise. In addition:

$$A = \begin{bmatrix} 0 & 0 & 0 & 0 \\ 0 & \dfrac{R_e C_e}{1 + R_e C_e} & 0 & 0 \\ 0 & 0 & \dfrac{R_p C_p}{1 + R_p C_p} & 0 \\ 0 & 0 & 0 & 1 \end{bmatrix}, B = \begin{bmatrix} R_\Omega \\ R_e \\ \dfrac{1}{1 + R_e C_e} \\ \dfrac{R_p}{1 + R_p C_p} \\ \dfrac{1}{C_{cap}} \end{bmatrix},$$

$$C_k = \left. \frac{\partial f(x_k)}{\partial x} \right|_{x = \hat{x}_{\bar{k}}}.$$

Then the standard EKF algorithm can be implemented.

III. EXPERIMENTAL VERIFICATION

Prior to the experiments, the battery is fully charged and subsequently discharged using a current=1C. The reference SOC is derived utilizing the method reported in [20], i.e., integrating the cell current with the time in post-process. The parameters in the equivalent circuit model of the investigated battery (TABLE I) can be obtained through Equ. (1) and *ZSimpWin* (section II. B.1), as listed in TABLE II.

A. Model Verification

In order to verify the capability of the proposed model in capturing the cell's electrical dynamic characteristics, a combined battery model incorporating the impedance-based equivalent circuit part and the OCV-SOC relationship part has been organized as depicted in Fig. 12. The terminal voltage V_0 is predicted by superimposing the dynamic potential produced by the equivalent circuit part (section II. B.1) and the OCV

TABLE II
THE MODEL PARAMETERS OF CIRCUIT FORMED AS
R(R(RC)(RC)(RC)) GIVEN BY ZSIMPWIN

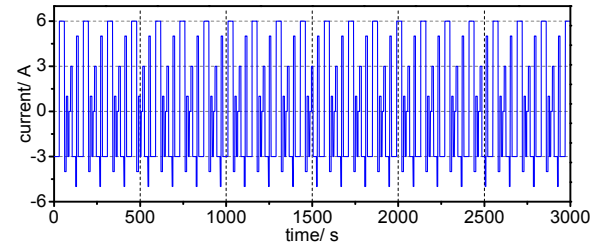| Component	Value	Component	Value
Cbulk(F)	30981	Rs(Ω)	0.0158
RΩ(Ω)	0.01	Cs(F)	0.5402
Rd(Ω)	$1.64 \cdot 10^8$	Rm(Ω)	0.01
Re(Ω)	0.01	Cm(F)	0.2446

Fig. 13. Self-designed alternating current profiles as simulated operating conditions.

generated by the reverse mapping from SOC to OCV according to the OCV-SOC relationship (section II. B.2).

The alternating current profiles used to simulate the operating conditions, as presented in Fig. 13, are both subject to the cell and the model with initial SOC=70 % and temperature=27℃.

In Fig. 14, although there exist discrepancies between the measured terminal voltage and the simulated response, the maximum error is kept within 25mV over the entire process and the underlying dynamic characteristics are essentially the same, which exhibits the excellent capability of the proposed model to track the electrical behavior of a battery.

B. Comprehensive Evaluation

The Federal Urban Driving Schedule (FUDS) and the Urban Dynamometer Driving Schedule (UDDS) [21], as shown in Fig. 15, are commonly used test cycles for EV research. In this section, a series of verification tests are conducted by applying FUDS and UDDS as simulated transient load sequences on the investigated cell to evaluate the feasibility of the proposed battery modeling approach and SOC estimation algorithm. For comparison, the EKF-based SOC estimation method described previously (section II. D) is
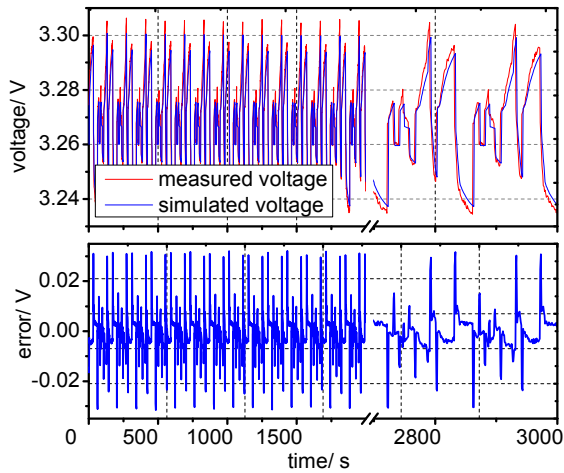
Fig. 14. The actual measurement and the simulated response to transient load profiles from SOC=70% and Temp=27℃.
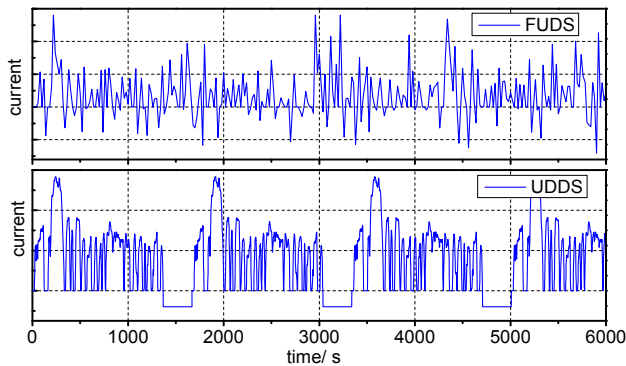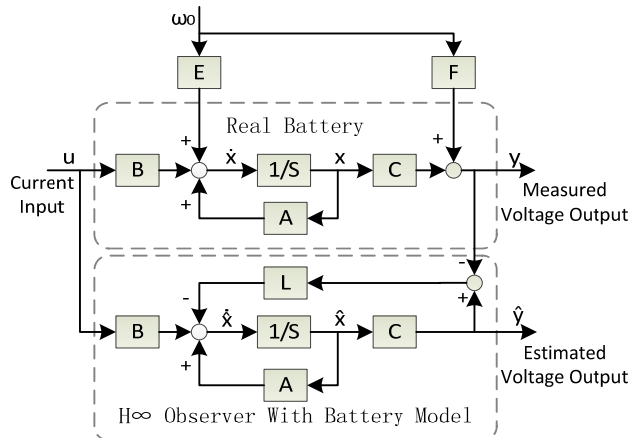

Fig. 15. FUDS and UDDS test cycles.

Fig. 16. Schematic diagram of H∞-based state observer.

implemented under the same test conditions.

By solving Equ. (23) with the MATLAB LMI toolbox, the attenuation level $\gamma > 0.7114$ is calculated. After many tests and design modifications, γ is set at 1.7114 considering the stability margin. The matrices P, X and L can be subsequently confirmed by solving LMI (22) as:

$$P = \begin{bmatrix} 8.3049 & -3.2952 & -3.5868 \\ -3.2952 & 6.9768 & -2.8611 \\ -3.5868 & -2.8611 & 6.3693 \end{bmatrix}, X = \begin{bmatrix} 1.0994 \\ 0.5945 \\ 1.5819 \end{bmatrix}$$

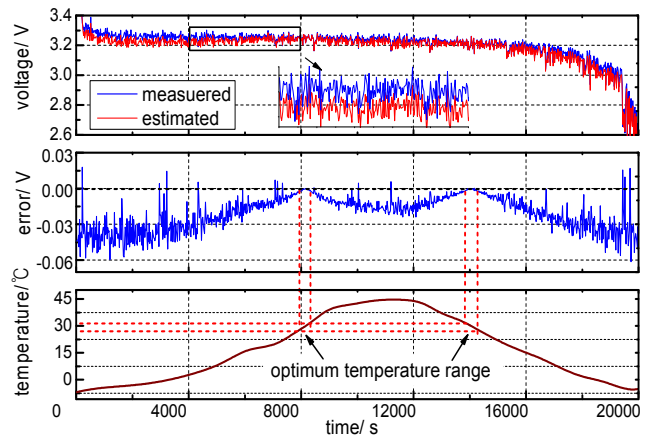$and\ L = P^{-1}X = [1.5156 \quad 1.5358 \quad 1.7917]^T.$

Fig. 17. Measured terminal voltage and estimated response V_0 (the output $\hat{y}$ of H∞ observer in Fig. 16) under FUDS cycles with varying ambient temperature (-7℃~43℃).

1) Terminal Voltage Prediction

Since the FUDS test cycle includes sharp rises and falls, it is suitable for examining the prediction capability of the designed observer which is constructed as expresed in Fig. 16. As observed from Fig. 17, by comparing the observer output with the actual battery terminal response, the estimated output is basically consistent with the measured output. In particular, the voltage deviation is close to zero within the optimum temperature range (29~32℃), which indicates the validity of the proposed H∞ observer.

2) SOC Estimation Considering Temperature

SOC estimation performance comparisons between the EKF-base method and the proposed method subject to the UDDS cycles with varying temperatures is shown in Fig. 18 (a). The estimation accuracies of both methods vary with the temperature. It is shown that the proposed estimator keeps a higher precision than the EKF-based estimator during the whole temperature range from -7℃ to 45℃. Especially, the proposed method gets the best result when the temperature is around the optimum temperature.

As shown in Fig. 18(a), it is clear that the temperature is a critical factor influencing estimation performance, especially at low temperatures. To analysis the robustness of the proposed method under harsh conditions, low temperature tests are conducted. Fig. 18(b) exhibits the estimation results with the temperature kept at 0℃. Compared with the EKF method, the proposed method has superior noise suppression capability. However, the performances of both methods degrade severely and there exist constant discrepancies of almost 2.199% (H∞) and 3.647% (EKF), respectively. This is due to the battery capacity fading and model parameter distortion arising from low temperatures. To concentrate on algorithm research, low temperature operation remains a future work that will be discussed in subsequent articles.

3) SOC Estimation with Current Sensor Bias

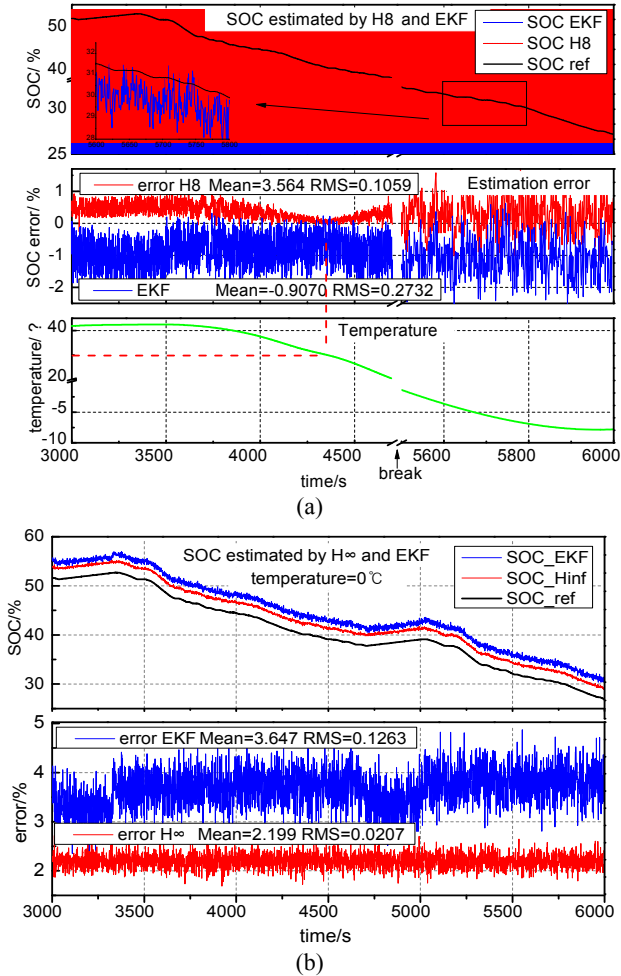In order to evaluate the robustness of the proposed method

Fig. 18. SOC estimation results by the proposed and EKF method under UDDS cycles (a) the ambient temperature varying from -7 to 43℃ (b) the temperature kept at 0℃.
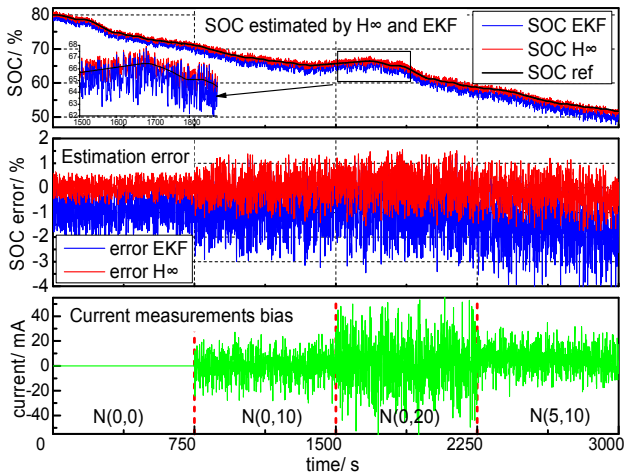

Fig. 19. SOC estimation results by the proposed and EKF method under UDDS cycles at 30℃, adding normally distributed bias $N(x, y)$ to the current measurements, where x, y indicate the mean and variance of the normal distribution.

against external noises, normally distributed random bias with different means and variances are injected into the current measurements. The experimental results under the

TABLE III
SOC ESTIMATION ERROR CHARACTERISTICS IN FIG. 19

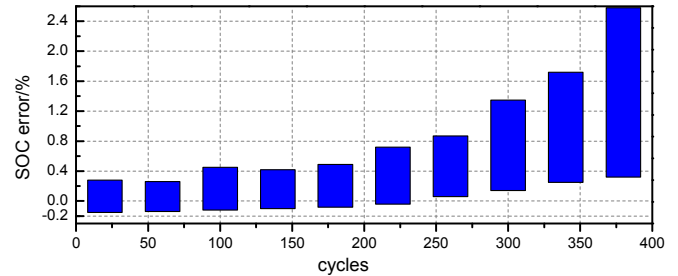| Bias characteristics	Error characteristics			
	Mean		RMSE	
	EKF	H∞	EKF	H∞
N(0,0)	-0.8979	0.0112	0.3509	0.0895
N(0,10)	-0.9638	0.0254	0.8073	0.3218
N(0,20)	-0.8823	0.0768	1.0603	0.4226
N(5,10)	-1.7037	-0.2157	0.8914	0.3505

Fig. 20. SOC estimation error margins vs. cycles, 30℃.

TABLE IV
SPECIFICATIONS OF 4 DIFFERENT LI-ION BATTERIES

	Bat1	Bat2	Bat3	Bat4
Manufacturer	HUANYU		FU NENG	SAM SUNG
chemistries	LiFePO$_4$		LiMn$_2$O$_4$	LiNi$_{1/3}$Co$_{1/3}$Mn$_{1/3}$O$_2$
Nominal capacity(Ah)	20	5	5	2.6
Nominal voltage(V)	3.2	3.2	3.6	3.7
Upper cut-off voltage(V)	3.65	3.65	4.2	4.2
Lower cut-off Voltage(V)	2.0	2.0	2.8	2.75
Operating temperature(℃)	Charge:0~45 Discharge: -20~60			

UDDS cycles in Fig. 19 show that the SOC can be accurately estimated with an error of less than 1.5% by the proposed method all over the process, and with an error of 4% by the EKF method as a comparison. Table III tabulates the statistical characteristics of the SOC estimation errors.

As observed from Table III, the negative impact on the performance of the EKF-based method resulting from measurement errors is more obvious, i.e., the proposed method is more tolerant to noises.

4) SOC Estimation Considering the Aging Factor

The aging effect is inevitable and increasingly severe as the number of charge-discharge cycles increases [22]. The cell is cycled repeatedly according to the electric vehicle profile (DST cycle) from full charge (3.65 V/cell) to 80% depth of discharge (DoD). The estimation error margins versus cycles are exhibited in Fig. 20. It is obvious that the performance can be maintained and remain below 0.5% when the cycle number is less than 200.
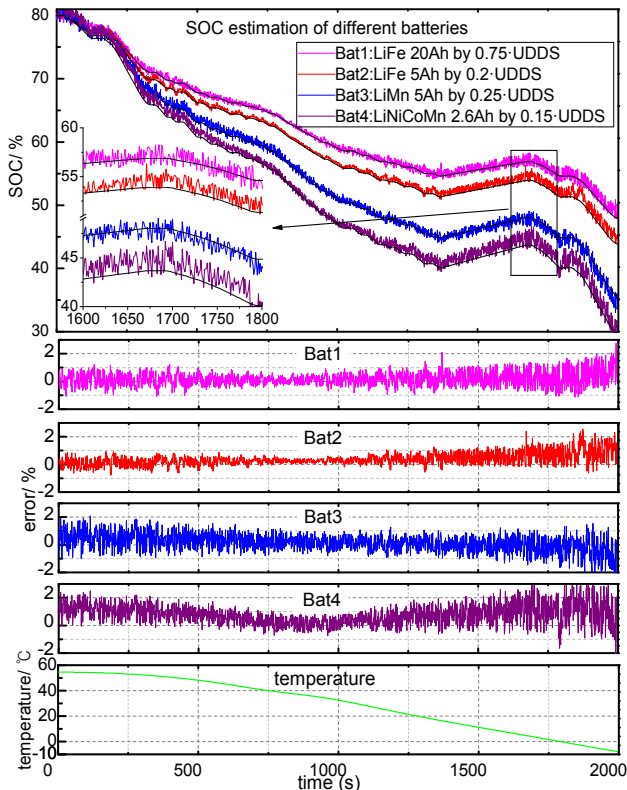
Fig. 21. SOC estimation results on four different Li-ion batteries by the proposed method under different magnifications of UDDS cycles with varying temperature.

C. Generalization Evaluation

In addition, the proposed method has also been applied to another four Li-ion batteries from different manufacturers and made of different cathode materials, as detailed in TABLE IV, to examine its generalization capability. To get roughly the same discharging trajectories, the batteries are subject to different magnifications of the UDDS cycles according to their capacities, e.g. 0.75•UDDS for Bat1 (20 Ah) and 0.15•UDDS for Bat4 (2.6 Ah). As can be seen in Fig. 21, the proposed estimator performs the best in the LiFePO$_4$ cases (Bat1 and Bat2) and the error is confined to 1.5% when the temperature ranges from 55℃ to 0℃. By comparison, there are a lot of sharp spikes for Bat3 (LiMn$_2$O$_4$) and Bat4 (LiNi$_{1/3}$Co$_{1/3}$Mn$_{1/3}$O$_2$). As the temperature drops, the estimation performances for all the four batteries degrade. In summary, for all the three types of Li-ion batteries the SOC error is confined to an acceptable level, less than 3% in most scenarios within the common operation temperature range, which is applicable to the real applications.

IV. CONCLUSION AND DISCUSSIONS

This paper develops an impedance-based equivalent circuit model by approximating the electrochemical impedance spectrum with RC-network circuits. In addition, the typical hysteresis phenomenon is modeled. Subsequently, a methodology incorporating the H∞ observer designated for OCV observation utilizing the equivalent circuit model and the hysteresis model developed for OCV-SOC mapping is proposed for SOC estimation. Validation experiments under complicated current profiles (FUDS and UDDS) together with varying temperatures and different current measurement bias are carried out. Besides, the influence of the aging factor is also evaluated. With the comparison of the EKF-based method, the proposed method provides better SOC estimation performance when there exist measurement errors and temperature fluctuations. In addition, generalization tests indicate that the proposed method is effective and applicable to other types of Li-ion batteries.

However, a few issues concerning the proposed method need to be discussed here. These issues can give directions for future work.

1) As the temperature falls below zero, the estimation performance degrades significantly. Hence, it is necessary to take temperature as a consideration when it goes beyond the range of [0,45]℃.

2) Aging is an important factor influencing estimation accuracy when the system works for a long time. To obtain more comprehensive models, the aging effect needs to be considered.

3) For batch applications, the identification of the OCV-SOC relationship is too complicated. More concise methods for establishing the OCV-SOC directly according to the parameters in product descriptions, such as chemistry, nominal capacity, nominal voltage, internal impedance and charge/discharge cut-off voltage, need to be developed.

REFERENCES

[1]   M. A. Roscher and D. U. Sauer, "Dynamic electric behavior and open-circuit-voltage modeling of LiFePO4-based lithium ion secondary batteries," *Journal of Power Sources*, Vol. 196, No. 1, pp. 331-336, Jan. 2011.

[2]   Y. He, X. T. Liu, C. B. Zhang, and Z. H. Chen, "A new model for state-of-charge(SOC) estimation for high-power Li-ion batteries," *Applied Energy*, Vol. 101, pp. 808-814, Jan. 2013.

[3]   S. Piller, M. Perrin, and A. Jossen, "Methods for state-of-charge determination and their applications," *Journal of power sources*, Vol. 96, No. 1, pp. 113-120, Jun. 2001.

[4]   K. S. Ng, C.-S. Moo, Y.-P. Chen, and Y.-C. Hsieh, "Enhanced coulomb counting method for estimating state-of-charge and state-of-health of lithium-ion batteries," *Applied energy*, Vol. 86, No. 9, pp. 1506-1511, Sep. 2009.

[5]   S. Lee, J. Kim, J. Lee, and B. H. Cho, "State-of-charge and capacity estimation of lithium-ion battery using a new open-circuit voltage versus state-of-charge," *Journal of power sources*, Vol. 185, No. 2, pp. 1367-1373, Dec. 2008.

[6]   P. Spagnol, S. Rossi, and S. M. Savaresi, "Kalman filter SOC estimation for Li-ion batteries," in *IEEE International*

Conference on Control Applications(CCA), pp. 587-592, Sep. 2011.

[7] M. Charkhgard and M. Farrokhi, "State-of-charge estimation for lithium-ion batteries using neural networks and EKF," *IEEE Trans. Ind. Electron.*, Vol. 57, No. 12, pp. 4178-4187, Dec. 2010.

[8] W. He, N. Williard, C. Chen, and M. Pecht, "State of charge estimation for electric vehicle batteries using unscented Kalman filtering," *Microelectronics Reliability*, Vol. 53, No. 6, pp. 840-847, Jun. 2013.

[9] B. Fridholm, M. Nilsson, and T. Wik, "Robustness comparison of battery state of charge observers for automotive applications★," in *19th World Congress*, Vol. 19, No. 1, pp. 2138-2146, Aug. 2014.

[10] X. Chen, W. Shen, Z. Cao, and A. Kapoor, "A comparative study of observer design techniques for state of charge estimation in electric vehicles," in *7th IEEE Conference on Industrial Electronics and Applications(ICIEA)*, pp. 102-107, Jul. 2012.

[11] X. Li, J. Jiang, C. Zhang, W. Zhang, and B. Sun, "Effects analysis of model parameters uncertainties on battery SOC estimation using H-infinity observer," in *IEEE 23rd International Symposium on Industrial Electronics(ISIE)*, pp. 1647-1653, Jun. 2014.

[12] D. D. Domenico, G. Fiengo, and A. Stefanopoulou, "Lithium-ion battery state of charge estimation with a kalman filter based on a electrochemical model," in *IEEE International Conference on Control Applications(CCA)*, pp. 702-707, Sep. 2008.

[13] H. He, R. Xiong, and J. Fan, "Evaluation of lithium-ion battery equivalent circuit models for state of charge estimation by an experimental approach," *Energies*, Vol. 4, No. 4, pp. 582-598, Mar. 2011.

[14] F. Huet, "A review of impedance measurements for determination of the state-of-charge or state-of-health of secondary batteries," *Journal of power sources*, Vol. 70, No. 1, pp. 59-69, Jan. 1998.

[15] M. Thele, O. Bohlen, D. U. Sauer, and E. Karden, "Development of a voltage-behavior model for NiMH batteries using an impedance-based modeling concept," *Journal of Power Sources*, Vol. 175, No. 1, pp. 635-643, Jan. 2008.

[16] A. A. H. Hussein, N. Kutkut, and I. Batarseh, "A hysteresis model for a lithium battery cell with improved transient response," in *26th Annual IEEE Applied Power Electronics Conference and Exposition(APEC)*, pp. 1790-1794, Mar. 2011.

[17] V. H. Johnson, A. A. Pesaran, and T. Sack, *Temperature-dependent battery models for high-power lithium-ion batteries*, City of Golden: National Renewable Energy Laboratory, pp. 1-17, 2001.

[18] I. Petersen, V. A. Ugrinovskii, and A. V. Savkin, *Robust Control Design Using H-∞ Methods*, Springer Science & Business Media, Chap. 3, 2012.

[19] J. Qiu, G. Feng, and J. Yang, "A new design of delay-dependent robust H-infinity filtering for discrete-time T-S fuzzy systems with time-varying delay," *IEEE Trans. Fuzzy Syst.*, Vol. 17, No. 5, pp. 1044-1058, Oct. 2009.

[20] Z. He, M. Gao, C. Wang, L. Wang, and Y. Liu, "Adaptive state of charge estimation for Li-ion batteries based on an unscented Kalman filter with an enhanced battery model," *Energies*, Vol. 6, No. 8, pp. 4134-4151, Aug. 2013.

[21] Dynamometer Driving Scheules Utilized at the National Vehicle and Fuel Emissions Laboratory, *http://www.epa.gov/nvfel/testing/dynamometer.htm*, Jun. 2012.

[22] G. Sarre, P. Blanchard, and M. Broussely, "Aging of lithium-ion batteries," *Journal of Power Sources*, Vol. 127, No. 1-2, pp. 65-71, Mar. 2004.

Jiale Xie received his B.S. degree from the Harbin Engineering University, Harbin, China, in 2010 and his M.S. degree in Control Science and Engineering from the Harbin Institute of Technology, Harbin, China, in 2012. From 2012 to 2013, he worked with the Envision Energy Co., Ltd., Shanghai, China, where he was in charge of the control strategies of wind turbines. Since 2014, he has been working towards his Ph.D. degree in the School of Astronautics, Harbin Institute of Technology. His current research interests include battery modeling and simulation, SOC and SOH estimation of power Li-ion batteries, series battery string equalization and embedded control.

Jiachen Ma was born in China, in 1964. He received his B.S., M.S. and Ph.D. degrees in Control Science and Engineering from the Harbin Institute of Technology, Harbin, China, in 1985, 1988 and 2006, respectively. He is presently working as a Professor in the School of Astronautics, Harbin Institute of Technology. His current research interests include intelligent robots, precise machine vision detection, embedded system applications and battery energy management.

Yude Sun was born in China, in 1964. He received his B.S. degree in Physics from Heilongjiang University, Harbin, China, in 1985 and his M.S. degree in Microelectronics and Solid State Electronics from the Harbin Institute of Technology, Harbin, China, in 1988. He is presently working as an Associate Professor at the Harbin Institute of Technology at Weihai. His current research interests include automotive electronics and embedded system applications.

Zonglin Li was born in China, in 1995. Since 2014, he has been working towards his B.S. degree in electrical engineering, from the Harbin Institute of Technology at Weihai, China. His current research interests include power electronics and embedded control.